01 Oct 2022

Benefits and Drawbacks of using Multiple Shrinkage Mitigating Strategies on Performance of Fiber-Reinforced Mortar

Kamran Aghaee

Kamal Khayat
Missouri University of Science and Technology, khayatk@mst.edu

Recommended Citation

K. Aghaee and K. Khayat, "Benefits and Drawbacks of using Multiple Shrinkage Mitigating Strategies on Performance of Fiber-Reinforced Mortar," *Cement and Concrete Composites*, vol. 133, article no. 104714, Elsevier, Oct 2022.
The definitive version is available at https://doi.org/10.1016/j.cemconcomp.2022.104714

Cement and Concrete Composites 133 (2022) 104714

Contents lists available at ScienceDirect

Cement and Concrete Composites

journal homepage: www.elsevier.com/locate/cemconcomp

Benefits and drawbacks of using multiple shrinkage mitigating strategies on performance of fiber-reinforced mortar

Kamran Aghaee, Kamal H. Khayat *

Department of Civil, Architectural and Environmental Engineering, Missouri University of Science and Technology, 500 W 16th Street, Rolla, MO, 65409, USA

ARTICLE INFO

Keywords:
Expansive agent
Factorial design
Internal curing
Microstructural analysis
Repair
Shrinkage reducing admixture
Superabsorbent polymer
Shrinkage mitigating strategies

ABSTRACT

Shrinkage mitigating strategies have been successfully used to prevent concrete cracking. Numerous studies have demonstrated the efficiency of shrinkage mitigating materials (SMM), such as expansive agent (EA), shrinkage reducing admixture (SRA), and superabsorbent polymer (SAP) on reducing shrinkage and cracking; however, few studies have addressed the limitations of using these materials. In addition, the mechanism of negative effect on microstructure and mechanical properties when these materials are used at high contents or in combinations is not well defined. This study investigates the effect of CaO-based EA, SRA, and SAP on compressive strength development, fiber pull-out strength, and shrinkage of fiber-reinforced mortar (FRM) mixtures. Hydration kinetics and internal relative humidity are also determined. Advanced microstructural characterization techniques are employed to explore the mechanism underlying the effect of SMM on the mechanical properties and shrinkage of FRM mixtures. Test results indicate that FRM made with coupled systems of SMM limited to 5% EA, 1% SRA, and 0.25% SAP are preferred. The preferred SMM combination considering compressive strength, fiber pull-out strength, and shrinkage is the coupled system made of EA and SRA. High heat of hydration obtained using 10% EA results in excessive portlandite formation and high expansion, which adversely affects the mechanical properties. The use of 0.5% SAP with additional internal curing water contributes to the excessive expansion of SAP particles and creation of voids into the matrix, which reduce compressive strength and fiber-matrix bonding. The results revealed that the individual use of 7.5% EA and coupled use of 5% EA either with 0.5% SRA or 0.125% SAP can result in producing flowable, high strength, and low shrinkage FRM mixtures applicable to repair.

1. Introduction

Shrinkage cracks can reduce the durability of concrete by providing a free path of deleterious substances into the depth of the concrete [1]. These cracks can induce freeze-thaw damage and accelerate the ingress of chloride ions into the concrete leading to the corrosion of reinforcing bars [2]. The corrosion products on reinforcing bars expand and propagate cracks resulting in lower effective concrete section, lower bonding between rebar and concrete, and eventually immature deterioration of the structure [3].

Different types of shrinkage (autogenous, chemical, plastic, drying, restrained shrinkage and etc.) are responsible for concrete cracking, which occur due to the moisture evaporation, capillary tension, surface tension, and disjoining pressure within the cement matrix [4]. The application of expansive agent (EA) [5], shrinkage reducing admixture (SRA) [6], and superabsorbent polymer (SAP) [7] can effectively mitigate the aforementioned types of shrinkage in concrete. However, there is evidence of shrinkage mitigating materials' (SMM) adverse effect on strength and durability of concrete when used beyond recommended dosages or in combination with other admixtures [8–14].

EAs by formation of calcium sulfoaluminate, calcium oxide, and magnesium oxide generate large amount of ettringite, portlandite, and brucite, respectively, which increase the solid phase of matrix. The compression exerted by the swelling of these hydration products counteracts the tensile stress by shrinkage. The challenges with using expansive agents in inhibiting shrinkage include the suitable occurrence time and expansion degree. The CSA-based EA (Type K EA) requires a lot of water for reaction, and may exhibit excessive or delayed expansion which can cause cracking and deterioration [15]. Shi et al. [12] reported that the use of 7.5% Type K EA can compensate for shrinkage by 50%, while it can increase the rate of rebar corrosion. Increase in transport properties of concrete such as air permeability, capillary absorption, and

* Corresponding author.
E-mail address: khayatk@mst.edu (K.H. Khayat).

https://doi.org/10.1016/j.cemconcomp.2022.104714
Received 3 June 2022; Received in revised form 31 July 2022; Accepted 4 August 2022
Available online 10 August 2022

chloride diffusion was reported, which was attributed to the excessive expansion of EA and microstructure. The application of MgO- and CaO-based require lower water for reaction. CaO-based EA expands quickly and can induce about 90% expansion at initial ages. Cement including 40% of MgO and supplementary cementitious materials, with good mechanical and durability properties were utilized in previous studies [16,17]. The use of lightly burnt MgO-based EA which is obtained through a calcination at 900–1300 °C (low temperature) is recommended over hard burnt MgO-based EA. The hard burnt MgO-based EA can react after setting of the concrete and exert delayed expansion and cracking [18].

SRA as a non-ionic surfactant, which includes amphiphilic molecules, reduces the surface tension of pore solution by over 50% and declines capillary stress, leading to lower shrinkage. Rajabipour et al. [8] studied the interactions between SRA and cement paste's pore solution. They reported that the accumulation of SRA in the pore solution drops the dissolution of alkali. Therefore, the alkalinity of the solution reduces and causes slower hydration, which explains delayed strength development [8]. Yang et al. [19] reported that the formation of SRA in pore solution is categorized into three types. In the first and second types, SRA is adsorbed on the solution-air and solution-solid interfaces, respectively, and both types effectively decrease shrinkage. In the third type, SRA dissolves in the pore solution. In this type, when SRA concentration is over critical micelle concentration, the aggregation of SRA occurs. This phenomenon is not in favor of the surface tension reduction, and adversely affects hydration of concrete. In addition, there is evidence that the inclusion of SRA can reduce air content and adversely affect freeze-thaw resistance of concrete. Therefore, it is crucial to comprehend the SMM's shrinkage mitigation mechanism and their interaction with each other.

SAPs are three-dimensional network polymers made of natural or synthetic monomers or pre-polymers, which are classified as ionic or non-ionic materials based on their chain nature [20,21]. SAP particles absorb and desorb up to 1500 g of water per g of SAP [22] depending on the relative humidity of the surrounding environment [23,24]. As the internal moisture of concrete is lost by hydration or external drying, the water inside the SAP particles is gradually infused into the matrix to avoid meniscus of capillary pores and self-desiccation [25,26]. SAPs are shown to be very effective in reducing self-desiccation and autogenous shrinkage, while they affect rheology and increase porosity [21]. The particles are subjected to expansion after water absorption and initial stetting, which can limit autogenous shrinkage cracking [22]. In addition, the adverse effect of SAPs on mechanical properties and the quality of aggregate/fiber interfacial transition zone (ITZ) is controversial [22,27]. Although they can promote hydration and densify the matrix [28,29] there is evidence of mechanical properties' degradation depending on SAP's utilized content, swelling rate, and the amount of generated porosity after their water release [30–34]. For example, De Meyst et al. [35] employed various types of SAPs with d_{50} of 10–100 μm and water absorption of 66–270 g/g. The strength reduction using 0.5% SAP was up to 68%. The authors reported that 0.5% of SAP with d_{50} of 40 and the lowest water absorption and swelling capacity slightly affected the cement hydration and exhibited the lowest reduction in 28d compressive strength (23%). Liu et al. used 0.2% SAP in combination with up to 7.5% EA and 1.5% SRA to mitigate shrinkage of ultra-high performance concrete (UHPC). The authors reported that the incorporation of SAP was more effective than SRA in enhancing the expansion of the UHPC made with EA. This was due to the water injection into the matrix by the SAP particles and higher hydration of EA. The use of SAP was shown to be less effective than SRA in mitigating drying shrinkage within six months. The reason was the increase in porosity by the SAP particles [36].

Although all the SMM are effective in reducing shrinkage and cracking, they can contribute to lowering mechanical properties and porosity of the cementitious material, at high contents or inefficient combinations. This study employs single or combination of various SMM to investigate their efficiency on slump, mechanical properties, shrinkage, and microstructural characteristics of FRM. A statistical factorial design was developed to evaluate the combined effect of CaO-based EA, SRA, and SAP on slump, compressive strength development, fiber pull-out, and shrinkage of FRM mixtures and determine the appropriate combinations. Hydration kinetics, internal relative humidity (IRH), XRD, and BSEM analysis were carried out to explore the mechanism underlying the effect of individual and combined SMM on the key characteristics of FRM mixtures. The study can provide insights into the design of crack-free FRM for the repair objectives. A multi-objective optimization based on slump, compressive and bonding strength, and shrinkage was performed to tailor the FRM for repair applications.

Table 1
Physical and chemical characteristics of cementitious materials.

	OPC	Type G EA
SiO_2, %	18.7	12.6
Al_2O_3, %	4.0	5.7
Fe_2O_3, %	3.6	1.9
CaO, %	65.9	82.6
MgO, %	1.7	0.1
SO_3, %	2.4	–
Na_2O eq., %	0.97	0.90
$CaCO_3$, %	3.3	–
LOI, %	1.5	–
Blaine fineness, m^2/kg	390	–
Density, g/cm^3	3.14	3.12

2. Experimental program

2.1. Materials

Ordinary portland cement (OPC), Type I/II conforming with ASTM C150, was used. A CaO-based (Type G) EA was utilized to compensate for shrinkage through initial expansion derived from the hydration of CaO. Table 1 presents the physical and chemical properties of the cementitious materials employed in this study.

Natural sand with fineness modulus of 2.6, specific gravity of 2.61, and water absorption of 0.36% was used. Straight steel fibers measuring 13 mm in length and 0.2 mm in diameter (aspect ratio of 65) were used. The fiber has a modulus of elasticity of 200 GPa and average tensile strength of 1200 MPa.

A non-ionic angular covalently cross-linked acrylamide SAP with a median particle size of 52.4 μm was utilized to provide IC. The SAP molecular weight (Mc value) between cross-links is about 1.3×10^5. Its water adsorption and desorption rates in filtered solution with w/cm of 5:1, simulating the pore solution [37,38], are 30 g/g and 95%, respectively. The particle size distribution of powder materials and aggregate and SAP water absorption and desorption are shown in Fig. 1. The mass of SAP adequate to compensate for early age shrinkage of the binder was determined using Eq. (1).

$$M_{SAP} = \frac{C_f \; CS \; \alpha_{max}}{S \; W_{SAP}} \tag{1}$$

where, M_{SAP} is the mass of dry SAP (kg/m^3), C_f is the binder content (kg/m^3), CS is the sum of early age shrinkage of cement. In this study, CS of 0.15 was applied, which was consistent with the early age shrinkage shown in section 3.4. α_{max} is the maximum expected degree of hydration (1), S is the absorption rate of SAP in filtrated pore solution, and W_{SAP} is the SAP desorption rate upon equilibrium at RH of 95%, expressed as a fraction of oven-dry mass [39].

A polycarboxylate-based high-range water reducer (HRWR) was utilized to enhance flowability. An SRA was used to mitigate shrinkage by reducing the surface tension of the capillary pores.

The mixing water of the mixtures was adjusted for the water content

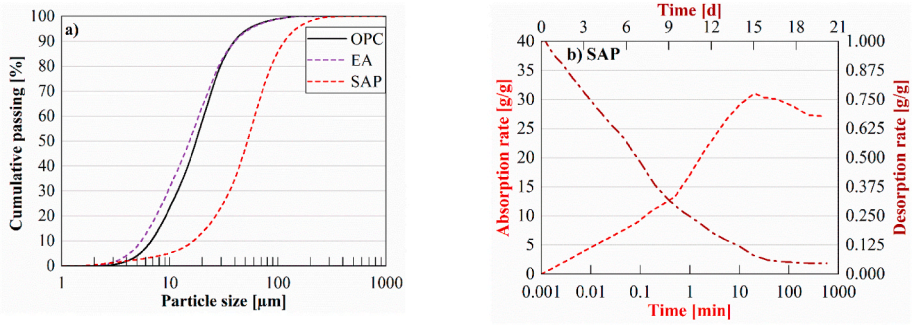

Fig. 1. (a) Particle-size distribution of OPC, EA, and SAP; (b) SAP absorption kinetics between 0 and 500 min and desorption kinetics between 1 and 20 days.

Table 2
Characteristics of chemical admixtures.

Admixture	Solid content (%)	Specific gravity
HRWR	34.0	1.05
SRA	15.0	1.10

in the HRWR and SRA, which corresponded to 66% and 85%, respectively. In the mixtures prepared with SAP, water was added to the mixing water at 30 g/g of SAP. Table 2 presents the characteristics of mentioned chemical admixtures.

2.2. Mixture proportioning

A factorial design approach was employed to evaluate the individual and combined effects of using EA, SRA, and SAP on compressive strength, fiber pull out bonding energy, and shrinkage of FRM mixtures. A total of 18 FRM mixtures were prepared, which are summarized in Table 3. In this study, w/cm and HRWR content were kept constant at 0.4 and 0.2% by mass of cement, respectively. The EA content corresponds to the substitution of cement by mass in percentage. The SRA and SAP contents correspond to the percentage mass of cement. The nomenclature of each mixture refers to the amount of EA, SRA, and SAP, respectively (e.g., 10EA2SRA0.5SAP denotes a cement paste mixture including 10% EA, 2% SRA, and 0.5% SAP). The REF mixture corresponds to the mixture made without any SMM.

For the factorial design, each factor was evaluated at minimum and maximum levels corresponding to two distinct coded values of −1 and +1, respectively. The first eight mixtures in Table 3, which represent 2^3 fractional factorial point mixtures, were defined based on the minimum and maximum coded values. In order to assess the experimental error of the derived models, replicated mixtures representing central points of the factorial design were set at coded values of zero. For the validation of the statistical models, the last six mixtures were designed using intermediate coded values. The difference between the absolute values and corresponding central point values divided by half of the range between the minimum and maximum absolute values corresponds to each coded value, as shown in Eq. 2.

$$\text{Coded EA} = (\text{Absolute EA} - 5)/5 \quad (2.1)$$

$$\text{Coded SRA} = (\text{Absolute SRA} - 1)/1 \quad (2.2)$$

$$\text{Coded SAP} = (\text{Absolute SAP} - 0.25)/0.25 \quad (2.3)$$

2.3. Mixing and curing

Five-liter batches of FRM using a Hobart mixer were prepared for each mixture. The mixing procedure was started with mixing the powder materials (OPC, EA, SAP) for 1 min. Sand was then introduced, and mixing continued for another 2 min. Afterward, water and HRWR were incorporated and mixed for 3 min. For mixtures containing SRA, the SRA was added following the mixing water and HRWR and mixed for 1 min. The mortar was maintained at rest for 2 min. At that time, before the incorporation of fibers, dog bone samples for fiber pull-out testing were cast. Finally, the steel fibers were added and the FRM was mixed at high speed for two more minutes. After mixing, samples for various experiments were prepared. The compressive strength samples were cast in

Table 3
Mixture combinations for factorial design.

	Mixture	Coded values			Absolute values		
		EA	SRA	SAP	EA	SRA	SAP
Fractional factorial points	REF	−1	−1	−1	0	0	0
	10EA	1	−1	−1	10	0	0
	2SRA	−1	1	−1	0	2	0
	0.5SAP	−1	−1	1	0	0	0.5
	10EA2SRA	1	1	−1	10	2	0
	10EA0.5SAP	1	−1	1	10	0	0.5
	2SRA0.5SAP	−1	1	1	0	2	0.5
	10EA2SRA0.5SAP	1	1	1	10	2	0.5
Central points	5EA1SRA0.25SAP	0	0	0	5	1	0.25
	5EA1SRA0.25SAP	0	0	0	5	1	0.25
	5EA1SRA0.25SAP	0	0	0	5	1	0.25
	5EA1SRA0.25SAP	0	0	0	5	1	0.25
Validation points	2.5EA1.5SRA0.17SAP	−0.5	0.5	−0.33	2.5	1.5	0.17
	2.5EA0.5SRA0.17SAP	−0.5	−0.5	−0.33	2.5	0.5	0.17
	2.5EA1.5SRA0.33SAP	−0.5	0.5	0.33	2.5	1.5	0.33
	7.5EA1.5SRA0.33SAP	0.5	0.5	0.33	7.5	1.5	0.33
	7.5EA1.5SRA0.17SAP	0.5	0.5	−0.33	7.5	1.5	0.17
	7.5EA0.5SRA0.33SAP	0.5	−0.5	0.33	7.5	0.5	0.33

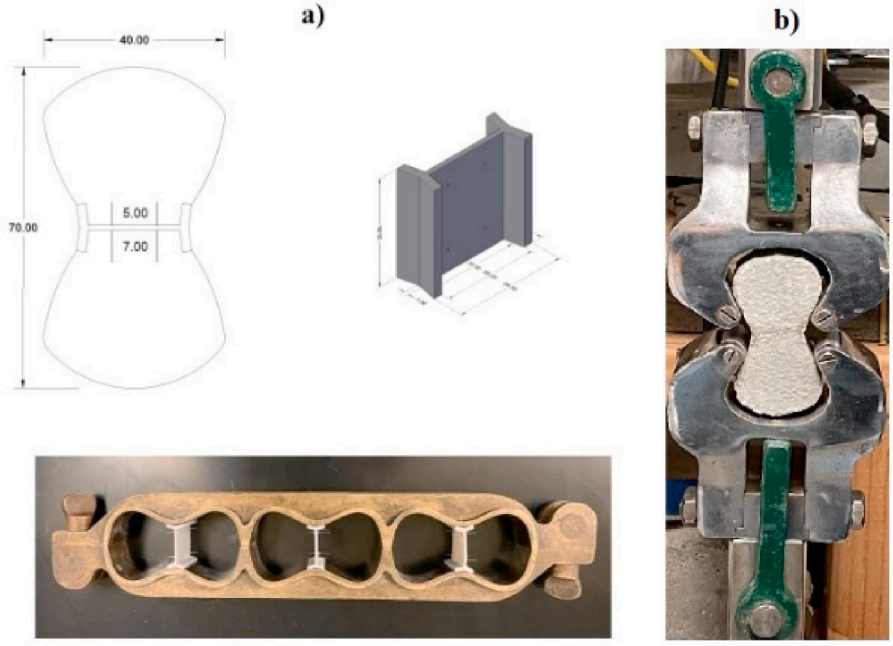

Fig. 2. (a) Schematic view of fiber pull-out sample, embedded plastic clip, and mold; (b) fiber pull-out by Instron universal testing machine.

one lift and shrinkage samples were cast in two layers. All the samples were consolidated by vibrating table. The molds were covered with a wet burlap and plastic sheet to prevent moisture loss. The samples were demolded after 24 h and stored in lime-saturated water tank at temperature of 23 ± 2 °C until 7 days. The shrinkage samples after demolding were covered with wet burlap and plastic sheet up to 7-day age, and then in ambient temperature of 21 ± 3 °C and 50% ± 5% relative humidity.

2.4. Testing method

2.4.1. Mini slump

Mini slump test was conducted according to ASTM WK63516 [40]. The cone was filled in two layers, and each layer was rodded 15 times. The sample was subjected to 15 jolts after the cone was lifted. The spread was measured in two perpendicular directions, and the average diameter was recorded.

2.4.2. Compressive strength

Compressive strength testing was performed using 50-mm cubes according to ASTM C109 [41] The samples were tested at 1, 7, and 28 days using a Tinius Olsen universal testing machine with a loading rate of 0.9 kN/s. The reported strengths represent the average of three to four samples.

2.4.3. Fiber pull-out

As shown in Fig. 2, fiber pull-out testing was performed on dog bone-shaped samples to evaluate fiber-matrix bonding. Four steel fibers were perpendicularly inserted into holes punched into plastic clip evenly spaced at 15 mm. The fibers were fixed to the holes using super glue. The clip was used to induce direct uniaxial tension at the interaction of fiber-matrix. A shorter fiber length (4 mm) was embedded into the pull-out half of the sample to ensure one side pull-out (Fig. 2). An Instron universal testing machine with a loading rate of 1 mm/min was used according to CECS13-2009 [42] (Fig. 2b). The bond strength was determined at 28 days using Eq. (3).

$$\tau_{max} = \frac{P_{max}}{n\pi dl} \tag{3}$$

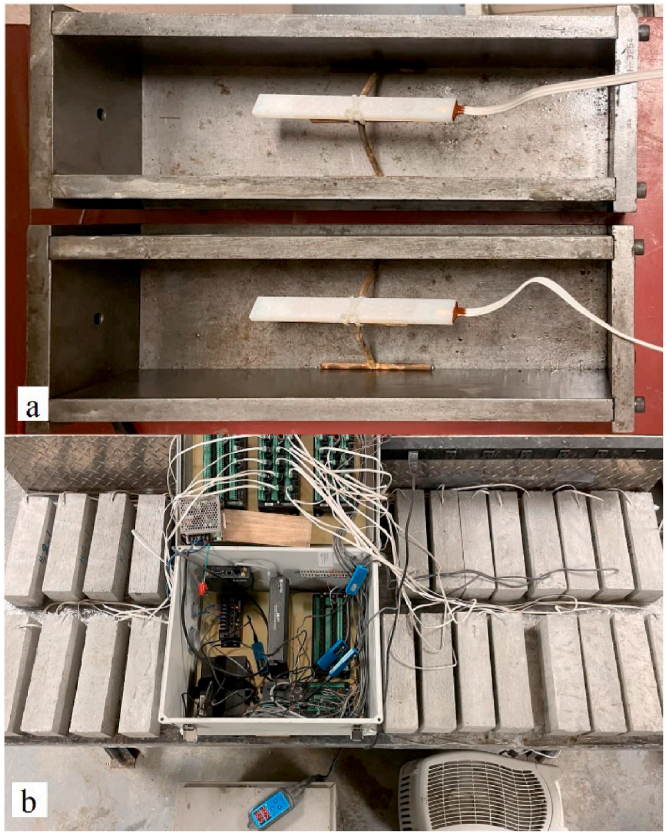

Fig. 3. (a) Shrinkage samples with 120 Ω strain gauges mounted on a chair located in the middle of mold; (b) strain gauges connected to DAQ.

where, τ_{max} (MPa) is the bond strength between the fiber and matrix at the maximum pull-out load; P_{max} (N) is the maximum pull-out load; n is the number of fibers; d (mm) is the diameter of a single fiber; and l (mm) is the embedment length of the fiber in pull-out half. The pull-out energy

Table 4
Initial slump spread of FRM mixtures.

Mixture	Slump spread (mm)
REF	215
10EA	205
2SRA	250
0.5SAP	185
10EA2SRA	165
10EA0.5SAP	170
2SRA0.5SAP	235
10EA2SRA0.5SAP	180

(N.mm) was obtained by calculating the area under the load-displacement curve.

2.4.4. Shrinkage

Shrinkage test was performed using 300 × 75 × 75 mm prismatic samples, as recommended by ASTM C157 [43]. As shown in Fig. 3a, for each sample a 120 Ω strain gauge with a gauge factor of 2.12 ± 0.5% was properly mounted on a small chair in the middle of the mold. The strain gauge was connected to a Campbell Scientific data acquisition system (DAQ) to collect strain measurements immediately after sampling up to 56 days (Fig. 3b).

2.4.5. Hydration kinetics

Mortar samples within 10 min after water to cement contact were inserted into I-Cal 8000 isothermal calorimeter. The calorimeter enabled the measurement of the rate and extent of heat release during the cement hydration in compliance with ASTM C1679. The test was conducted in isothermal condition at temperature of 20 °C. The heat flow (mW/g_{cement}) and heat of hydration (J/g_{cement}) were calculated for 48 h.

2.4.6. Internal relative humidity (IRH)

Immediately after casting the shrinkage prisms, a copper tube with 10 mm dimeter and 45 mm length which were sealed with duct tape at the bottom were inserted into the fresh concrete. The center of the tube was located at 37.5 mm from the FRM sample sides. Then, the mortar around the tube was externally vibrated and squeezed to make sure that the tube was surrounded by FRM before IRH sensor was slid through the copper tube. Finally, the upper part of the tube was sealed with silicon. The IRH was then connected to a laptop and RH was recorded every minute by data acquisition software.

2.4.7. XRD analysis

Additional 50-mm cube samples were prepared for microstructure testing. After 28 days, the samples were crushed and soaked in isopropyl alcohol to stop cement hydration. The samples were then oven dried at 60 °C for 24 h before testing. Up to 5 g of crushed particles were ground to powder with fines passing through the 75 μm sieve before use for XRD analysis. A Philips MPD X-ray diffractometer to characterize crystalline phases of FRM mixtures at 2θ values ranging from 5° to 90° and scanning rate of 1.5°/min was employed for testing.

2.4.8. Backscattered electron microscopy (BSEM)

The BSEM was utilized to investigate the morphology of the FRM samples at the interface of fibers. The chemical element mapping was used to determine the distribution of various elements at the fiber-matrix interface. For this test, samples measuring about 35 × 35 mm were cut using a diamond saw blade from intact 50 × 50 mm FRM cubes and dried overnight at 110 °C before mounting in epoxy. The samples were then soaked in epoxy. While the epoxy was still fluid, a vacuum was applied for about 10 min. Afterward, samples were polished with 220–4000 grit pads prior to the application of diamond paste as the final polish. After polishing, the samples were gold-coated using Denton desk V standard sputter coater. A Tescan VEGA3 scanning electron microscope with back-scattered detector in high vacuum mode was applied for BSEM testing.

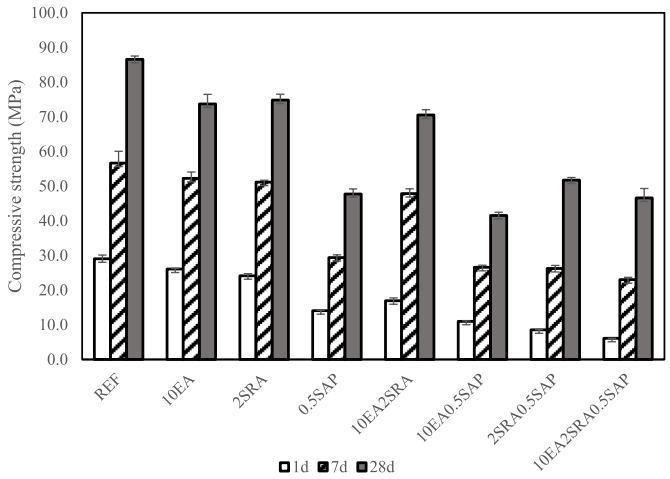

Fig. 4. Compressive strength development of FRM mixtures.

3. Result and discussion

3.1. Mini slump

Table 4 summarizes the mini slump spread of the investigated mixtures used for the factorial design, here referred to as the main mixtures. The initial slump values ranged between 165 and 250 mm, with the 2SRA and 10EA2SRA mixtures representing the highest and lowest values, respectively. The addition of EA and SAP reduced the mini slump flow by 5% and 14%, while the use of SRA increased it by 16%. The reducing effect of EA can be attributed to the quick chemical reaction of the CaO in EA and formation of CH [44,45]. The slump reduction observed in mixtures made with SAP, despite the additional water used during mixing, can be related to the rapid water absorption and swelling of the SAP particles. Dang et al. [46] reported a decrease in mini slump when dry SAP was used at 0.2% or higher content, by mass of cement. The coupled use of EA-SRA or EA-SAP, and combined use of all SMM resulted in lower slump spread at about 170 mm. However, the coupled use of SRA-SAP exhibited 9% higher mini slump compared to the REF. This workability enhancement can be attributed to the positive effect of SRA on viscosity of the pore solution and its delaying effect on hydration [47,48].

3.2. Compressive strength

Fig. 4 illustrates the compressive strength development of the main mixtures at 1, 7, and 28 days. The 28-d compressive strength ranged between 42 and 87 MPa. The highest and lowest strengths at 28-d age were recorded for the REF and 10EA0.5SAP mixtures, respectively. Using either EA or SRA and their combination reduced the compressive strength to 70–75 MPa. The use of SAP resulted in dramatic strength reduction (42–52 MPa at 28-d). The high absorption rate and swelling of the SAP particles can lead to the formation of macro-voids in the matrix and strength reduction [49].

Although the incorporation of EA resulted in faster strength development compared to the SRA during the 7-day period of moist curing, the final strength of mixtures including SRA was up to 25% higher than those made with EA. The quick strength development of mixtures made with EA within moist curing duration indicates the importance of water for the reaction of EA and CH formation [50,51]. On the other hand, the slow strength development of FRM made with SRA is associated with reducing the surface tension of capillary pores and evaporation water loss [8,52–54]. At early stages, SRA concentrates in pore solution can retard the hydration of cementitious materials and lowers the

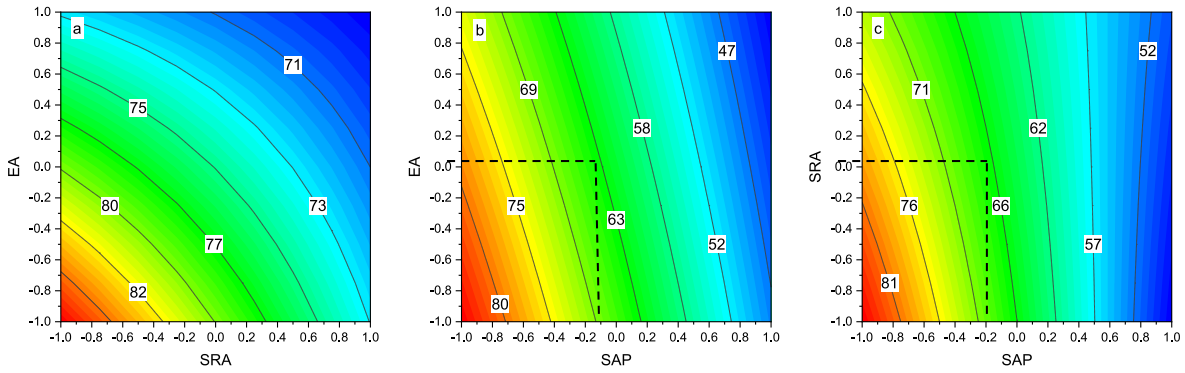

Fig. 5. Contour diagrams presenting coupled effect of (a) EA and SRA; (b) EA and SAP; (c) SRA and SAP on 28-d compressive strength of FRM mixtures (Note: the third factor is held at coded values of −1).

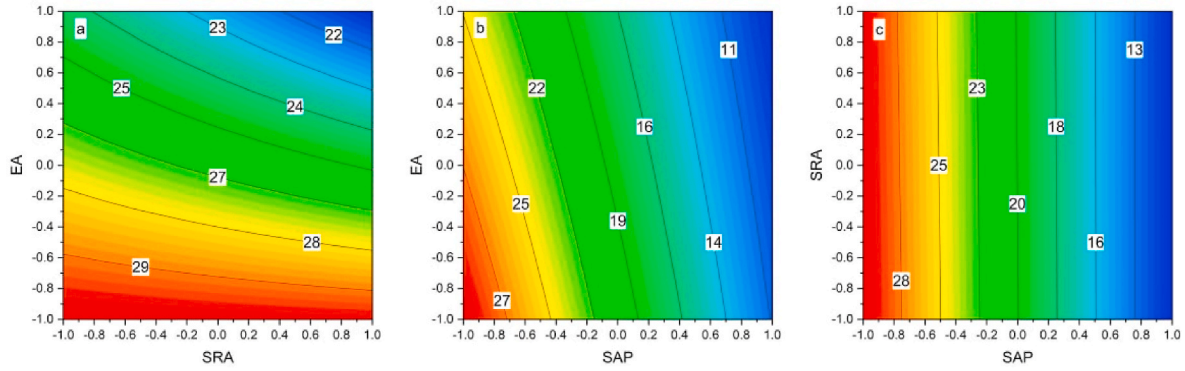

Fig. 6. Contour diagrams presenting coupled effect of (a) EA and SRA; (b) EA and SAP; (c) SRA and SAP on 28-d fiber pull-out strength (Note: the third factor is held at coded values of −1).

Table 5
Fiber pull-out peak load and energy at 28 days.

Mixture	Peak Load (N)	Bond strength (MPa)	Energy (N.mm)
REF	250	31	104
10EA	216	26	98
2SRA	230	28	92
0.5SAP	96	12	51
10EA2SRA	183	22	83
10EA0.5SAP	85	10	48
2SRA0.5SAP	91	11	56
10EA2SRA0.5SAP	87	11	62

portlandite formation [55]. The incorporation of both EA and SRA resulted in slightly lower strength compared to the mixtures made with the individual EA/SRA, especially within the first week.

Contour diagrams demonstrating the coupled effect of SMM on the 28-d compressive strength are shown in Fig. 5. It is worth mentioning that the data associated with the contour plots were obtained from JMP software and plotted using OriginPro 2022. The increase in SMM content reduced compressive strength; the usage of SAP presented the greatest effect on strength reduction. Fig. 5a shows that the coupled use of EA and SRA resulted in the lowest drop in strength—around 15% at the highest contents. The coupled use of SRA-SAP and EA-SAP are not recommended at high dosages, however, at coded values of zero (i.e., 5% EA, 1% SRA, and 0.25% SAP) it can lead to 28-d compressive strength higher than 60 MPa (Fig. 6b and c).

3.3. Fiber pull-out

Table 5 summarizes the results of fiber pull-out testing on the main FRM mixtures at 28 days. The highest and lowest fiber pull-out characteristics were exhibited by the REF and 10EA0.5SAP mixtures, respectively. The individual use of 10% EA diminished the bond strength and pull-out energy of FRM by 14% and 6%, respectively. Guo et al. [56] reported that the use of 10% CSA based EA can reduce the fracture energy of concrete with a strength order of 25 MPa and w/cm of 0.47, up to 60 days. The excessive unrestrained expansion and the presence of microcracks caused the drop in fracture energy. The negative effect of individual use of 2% SRA was insignificant (10%) on fiber pull-out characteristics. However, the use of 0.5% SAP significantly dropped the bond strength and pull-out energy of FRM by 61% and 51%, respectively. Although the combined use of SMM degraded the FRM's bond strength and pull-out energy by 66% and 54%, respectively, the lowest degradation could be obtained by the combination of EA and SRA.

Fig. 6 illustrates contour diagrams for the coupled effect of SMM on 28-d fiber pull-out strength of the FRM mixtures. As shown, the increase in SMM content diminished the 28-d fiber pull-out strength. SAP presented the highest and SRA the lowest effect on the strength reduction. The vertical contours in Fig. 6c indicate that the effect of SAP is very dominant compared to SRA on the strength reduction. Fig. 6a shows that the coupled use of EA and SRA resulted in the lowest strength reduction—around 25% using the highest contents. The coupled effect of SRA-SAP is barely preferred to EA-SAP. These combinations are not recommended at the highest ratios, however, using them at the coded value of zero—5% EA, 1% SRA, and 0.25% SAP—leads to 28-d fiber pull-out strength around or over 20 MPa.

3.4. Shrinkage

In order to compare the volume change, shrinkage profiles of the

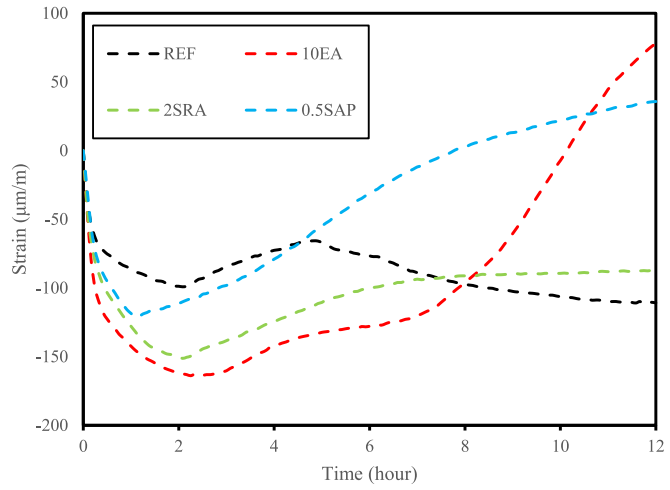

(a)

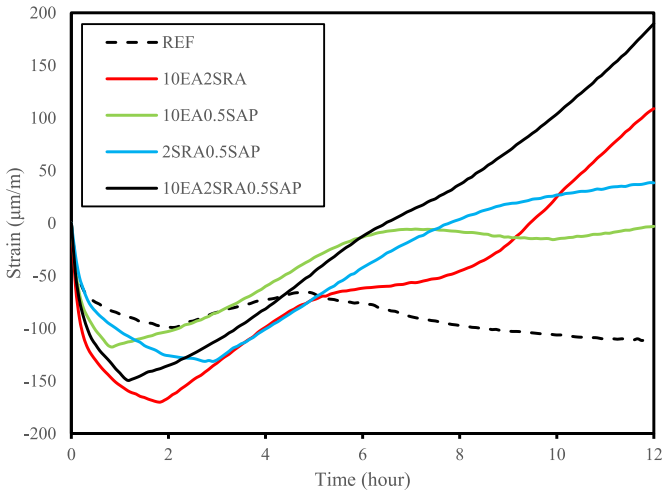

(b)

Fig. 7. Early age shrinkage strain of FRM mixtures made with (a) single SMM; (b) combination of SMM, at early ages.

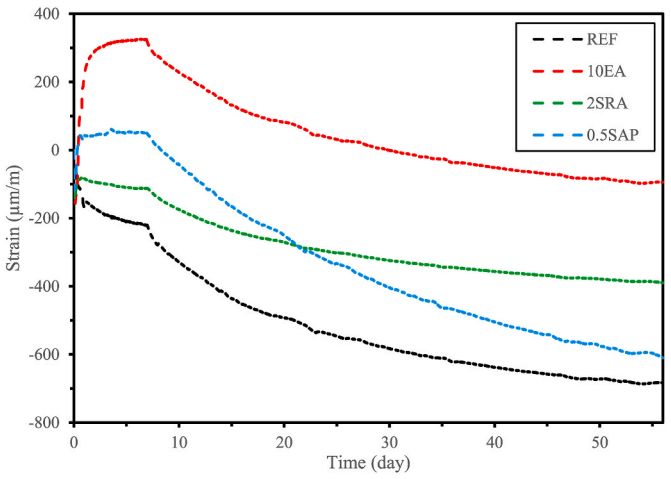

(a)

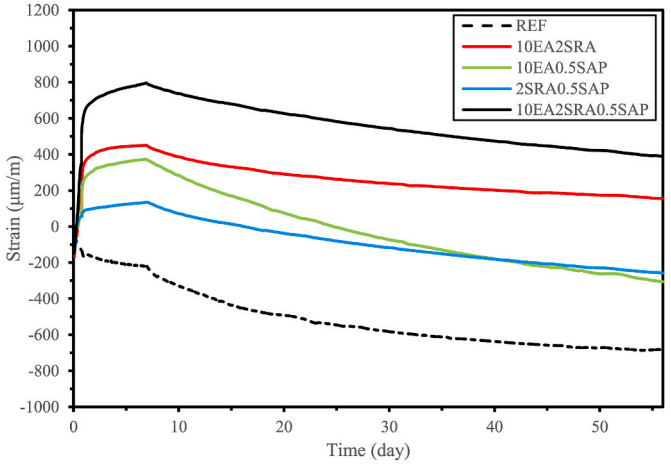

(b)

Fig. 8. Shrinkage strain of FRM mixtures made with (a) single SMM; (b) combination of SMM, up to 56 days.

main FRM mixtures made with different SMM are plotted in Figs. 8 and 9. Fig. 8a and b shows early age shrinkage up to 12 h. As shown, the lowest and highest early age shrinkage up to 4 h was demonstrated by the REF and 10EA mixtures; however, at 12 h the trend switched. The 2SRA and 0.5SAP mixtures presented the mediocre early age shrinkage range. Fig. 7b shows that the mixtures made with the combination of 10% EA and 2% SRA, 10EA2SRA, and 10EA2SRA0.5SAP showed the highest and lowest shrinkage within the first 2 h and at 12 h, respectively. This high and immediate shrinkage could be due to the absorption of water by EA, and the following initial expansion was a result of EA hydration and CH formation. The combined use of EA-SAP and SRA-SAP totally compensated for the early age shrinkage at 12 h.

Fig. 8a and b shows the shrinkage of main mixtures up to 56 days, ranged from 680 μm/m shrinkage for the REF mixture to 390 μm/m expansion for the 10EA2SRA0.5SAP mixtures. Fig. 8a shows that, during the moist curing, the highest expansion of 320 μstrain among the individual systems was recorded for the 10EA mixture, which led to insignificant shrinkage (90 μstrain) at 56 days. The use of 2% SRA did not cause any expansion, while it significantly mitigated the shrinkage rate and resulted in about 390 μstrain shrinkage at 56 days. A previous study by Collepardi et al. [57] indicated that, under dry curing after 36 h, the use of 1.15% SRA caused almost no expansion, while the shrinkage trend was mitigated considerably and led to 300 μm/m final shrinkage after a month. The use of 0.5% SAP caused negligible expansion (40 μstrain) and reduced shrinkage of the 0.5SAP mixture by 70 μstrain compared to the REF mixture. Although the 0.5SAP mixture was not very effective in reducing the drying shrinkage, a previous study by Aghaee et al. [58] using the same SAP in cement paste indicated significant effect on autogenous shrinkage reduction. The results of the study showed that the autogenous shrinkage of reference mixture made without any shrinkage mitigating strategies (700 μm/m at 28 days) can be eliminated using 0.5% SAP. The insignificant effect of SAP on this study can be associated with swelling of the SAP beyond the ideal range of 100–200 μm [38]. The excessive swelling retains large pores after desorption, which contributes to drying shrinkage at later ages. Thus, this SAP cannot be an ideal one to reduce drying shrinkage. As shown in Fig. 8b, the combination of 10% EA and 2% SRA amplified the effect and caused the highest expansion during the moist curing for the 10EA2SRA and 10EA2SRA0.5SAP mixtures. Although half of the initial expansion depressed, the mixtures showed over 150 μstrain expansion at 56 days. The 10EA0.5SAP and 2SRA0.5SAP mixtures presented a mediocre shrinkage strain range and converged at strain of about −280 μm/m after 56 days. Corinaldesi [59] used 10% CaO-based EA and 1% SRA, by mass of cement, in self-consolidated concrete. It was reported that the

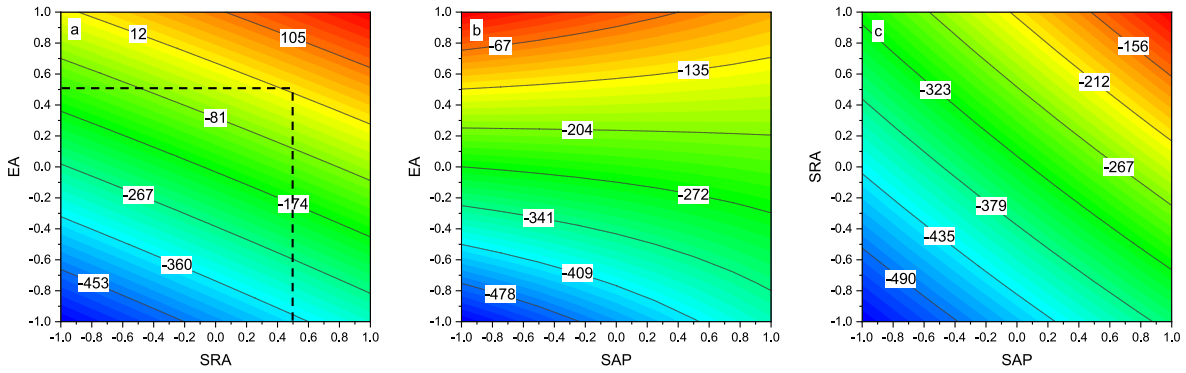

Fig. 9. Contour diagrams presenting coupled effect of (a) EA and SRA; (b) EA and SAP; (c) SRA and SAP on 28-d shrinkage (Note: the third factor is held at coded values of −1).

Table 6
Compressive strength, fiber pull-out energy, and shrinkage strain of investigated FRM mixtures.

No.	Mixture	Slump (mm)	Compressive strength (MPa)	Fiber pull-out strength (MPa)	Shrinkage strain (μm/m)
		Initial	28d	28d	28d
1	REF	215	87	31	−567
2	10EA	205	74	26	14
3	2SRA	250	75	28	−316
4	0.5SAP	185	48	12	−377
5	10EA2SRA	165	71	22	247
6	10EA0.5SAP	170	42	10	−46
7	2SRA0.5SAP	235	52	11	−104
8	10EA2SRA0.5SAP	180	47	11	558
9	5EA1SRA0.25SAP	200	60	16	−184
10	5EA1SRA0.25SAP	190	58	17	−123
11	5EA1SRA0.25SAP	195	59	12	−61
12	5EA1SRA0.25SAP	195	60	15	−123
13	2.5EA1.5SRA0.17SAP	205	65	24	−140
14	2.5EA0.5SRA0.17SAP	210	69	25	−208
15	2.5EA1.5SRA0.33SAP	195	56	18	−38
16	7.5EA1.5SRA0.33SAP	190	51	16	67
17	7.5EA1.5SRA0.17SAP	200	63	17	17
18	7.5EA0.5SRA0.33SAP	185	55	12	−8

Table 7
Derived statistical models for different properties at 95% confidence level (based on coded values).

Property	Derived equation	R^2	p-value
Slump (mm)	−18.9 EA – 13.4 EA.SRA – 9.0 SAP + 7.4 SRA.SAP + 198.7	0.84	<0.001
28-d compressive strength (MPa)	−14.7 SAP – 3.5 EA + 2.9 SAP (SRA - 0.05) + 60.6	0.97	<0.001
28-d fiber pull-out strength (MPa)	−8.2 SAP – 2.3 EA + 18.0	0.88	0.0007
28-d shrinkage (μm/m)	246.5 EA + 158.7 SRA +79.5 SAP - 86.1	0.90	<0.001

addition of EA was more effective than SRA in the initial expansion and final shrinkage compensation. The combination of EA and SRA caused stronger initial expansion, which gradually reduced while it remained positive after 60 days.

Contour diagrams in Fig. 9 show the coupled effect of SMM on 28-d shrinkage of FRM mixtures. As mentioned, all the SMM considerably improved shrinkage. The direction of the contour lines indicates that EA demonstrated the highest and SAP the lowest influence on 28-d shrinkage. As shown in Fig. 9a, the coupled use of either EA and SRA at the coded value of 0.5 can result in a free-shrinkage FRM at 28 days. According to Fig. 9b, high content of EA (around coded value of one) coupled with SAP at coded values of less than zero could result in insignificant or non-shrinkage FRM at 28 days. Fig. 9c indicates that employing a coupled system of SRA-SAP cannot lead to non-shrinkage FRM after 28 days.

Table 6 listed the values of compressive strength, fiber pull-out energy, and shrinkage at 7 and 28 days for all the investigated mixtures, which applied for the factorial design modeling.

3.5. Factorial design analysis

3.5.1. Derived statistical models

The derived statistical models for compressive and fiber pull-out strength and shrinkage of cement paste are presented in Table 7. The statistical responses indicated the significant effect of EA, EA-SRA, SAP, and SRA-SAP on initial slump; SAP, EA, and SRA-SAP on 28-d compressive strength; SAP and EA on 28-d fiber pull-out strength; EA, SRA, and SAP on 28-d shrinkage of FRM mixtures.

3.5.2. Multi-objective mixture optimization

A numerical optimization method was employed in which statistical responses, goals, and significance of the properties were applied to determine the desirability factors. The JMP statistical software was used with desirability functions for various selected goals [60,61]. As mentioned, workability, compressive strength, bonding, and shrinkage are the main challenges in repair concrete. Therefore, four key material properties including slump, 28-d compressive strength, 28-d fiber pull-out strength (MPa), and 28-d shrinkage were considered to optimize the SMM for the repair concrete. Based on the objective of this study, achieving relatively high slump, high mechanical characteristics, and low shrinkage after 28 days were targeted, as shown in Table 8. The

Table 8
Criteria for mixture optimization.

No.	Material property	Goal	Low limit	High limit	Importance
1	Slump (mm)	Match Target	160	260	1
2	28-d compressive strength (MPa)	Maximize	40	90	3
3	28-d fiber pull-out strength (MPa)	Maximize	10	32.5	2
4	28-d shrinkage (μm/m)	Match Target	−600	600	3

Table 9
Optimized mixtures with high overall desirability values.

Coded value			Absolute value (%)			Desirability index
EA	SRA	SAP	EA	SRA	SAP	
0.5	−1	−1	7.5	0	0	0.77
0	−0.5	−1	5.0	0.5	0	0.71
0	−1	−0.5	5.0	0	0.125	0.60

Table 10
Characteristics of optimized mixtures.

Optimized mixtures	Slump (mm)	28-d compressive strength (MPa)	28-d fiber pull-out strength (MPa)	28-d shrinkage (μm/m)
7.5 EA	206	76	26	−136
5EA0.5SRA	208	78	27	−218
5EA0.125SAP	201	71	23	−258

Table 11
Cumulative heat of hydration for FRM mixtures over 48 h of hydration.

Mixture	Heat of hydration (J/g_{cement})			Difference vs. REF at 48 h
	12 h	24 h	48 h	
REF	82.4	179	231	100%
10EA	118	207	254	110%
2SRA	62.6	162	218	94%
0.5SAP	80.9	180	236	102%
10EA2SRA	91.2	162	238	103%
10EA0.5SAP	109	204	260	113%
2SRA0.5SAP	61.5	160	223	97%
10EA2SRA0.5SAP	87.8	186	241	104%

goal "Match Target" supports the objectives with default target values midway between lower and upper limits [61]. The low and high limits refer to the minimum and maximum values, respectively, within the modeled range of properties.

After applying the optimization criteria in JMP, a desirability index (d_i) ranging from 0 to 1 for each property was obtained. The overall desirability index (D), which represents the overall performance of the cement paste considering all the properties in Table 8 was analyzed based on Eq. (4) [61].

$$D = \left(\prod_{i=1}^{4} d_i^{r_i}\right)^{\frac{1}{\sum r_i}} \quad (4)$$

where, i is the number of property (Table 8), d_i is the desirability index, and r_i indicates the importance of the property.

The overall desirability index was utilized to select three candidate mixtures, as presented in Table 9. The table indicates that the individual use of 7.5% EA and coupled use of 5% EA either with 0.5% SRA or 0.125% SAP leads to high overall desirability ranging from 0.60 to 0.77.

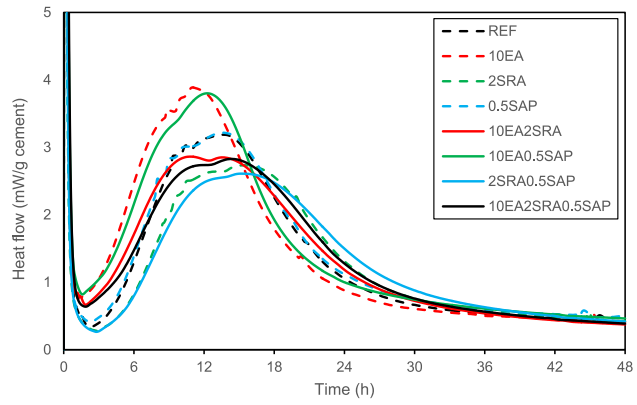

(a)

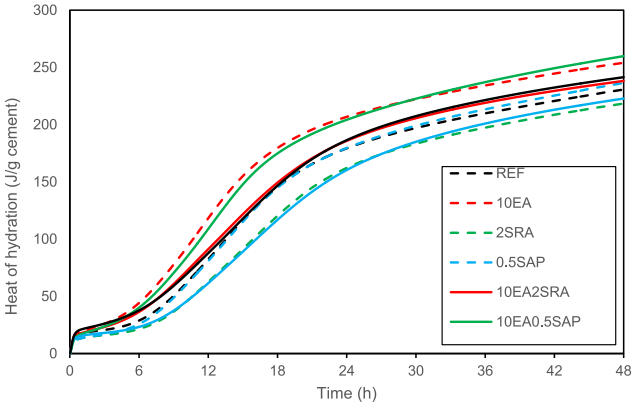

(b)

Fig. 10. (a) Heat flow; (b) cumulative heat evolution of FRM mixtures.

Table 10 presents the predicted characteristics of these mixtures. The results indicate that the optimized mixtures would provide relatively high slump, high compressive and fiber pull-out strength, and low shrinkage after 28 days. Regarding the required workability, mechanical properties, bonding, and shrinkage characteristics for repair purpose, these mixtures would serve as proper candidates.

3.6. Hydration kinetics

Table 11 summarizes the cumulative heat of hydration for the main FRM mixtures up to 48 h. The presence of EA led to increasing the heat of hydration. The highest cumulative heat of hydration was exhibited by the 10EA and 10EA0.5SAP mixtures—up to 13% higher than the REF mixture. On the other hand, the use of SRA reduced the heat of hydration, and the lowest cumulative heat of hydration was recorded for the 2SRA and 2SRA0.5SAP mixtures—up to 6% lower than the REF mixture. Comparing the effect of EA and SRA on heat of hydration justifies the prompt early age strength development and expansion of mixture prepared with EA compared to SRA presented in sections 3.1 and 3.3. The use of SAP slightly increased the heat of hydration. This could explain higher initial expansion of SAP-included mixtures versus the counterpart. The cumulative heat of hydration for the 10EA2SRA0.5SAP mixture was higher than those of the 2SRA and 0.5SAP mixtures, and lower than that of the 10EA mixture.

In order to better understand the effect of SMM on the performance, the heat evolution of main FRM mixtures is plotted in Fig. 10a and b. It is shown that the 10EA and 10EA0.5SAP mixtures exhibited the shortest induction period and highest peaks afterward. The enhanced heat evolution promoted portlandite (CH) generation and contributed to high

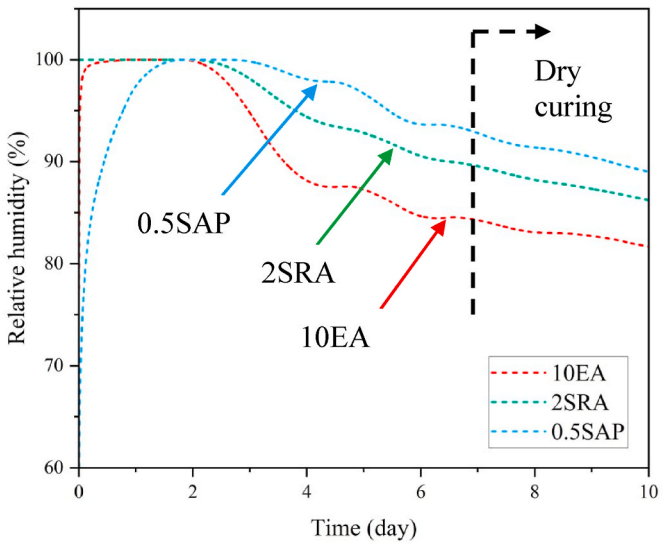

Fig. 11. Relative humidity change of FRM mixtures with single SMM.

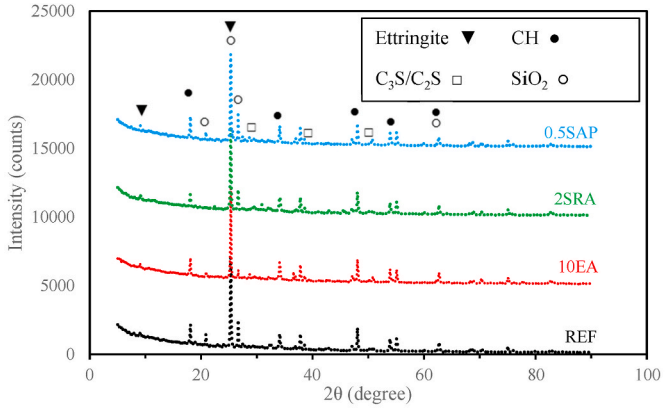

(a)

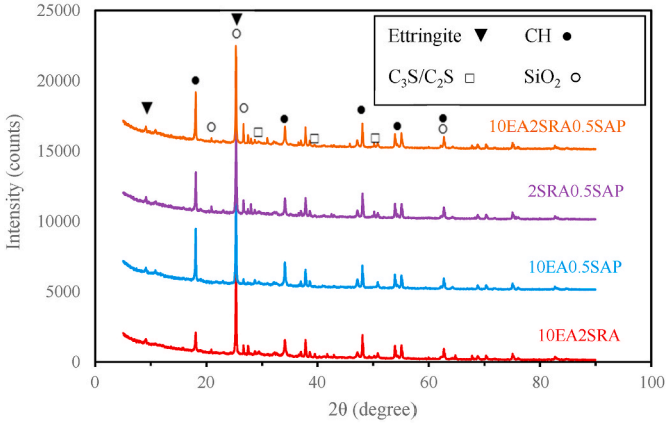

(b)

Fig. 12. XRD pattern of FRM mixtures made with (a) single SMM; (b) combination of SMM, at 28 days.

initial expansion of these mixtures, as observed in section 3.4 (Fig. 7a and b). The mentioned mixtures also presented a relatively short acceleration/deceleration stage, which resulted in quick loss of the expansion, especially for the 10EA0.5SAP mixture (see Fig. 7b). The delayed induction period, lowest peak of heat flow, and wide acceleration/deceleration stage presented by the 2SRA and 2SRA0.5SAP mixtures explain the lower cumulative heat of hydration, delayed strength development, and insignificant expansion of these mixtures as discussed in 3.2 and 3.4.

Table 12
Semi-quantitative analysis of crystalline phases for FRM mixtures at 28 days.

Mixture	Crystalline phase (%)			
	Ettringite	CH	C_3S/C_2S	SiO_2
REF	3.5	13.2	6.0	14.3
10EA	2.8	19.3	5.5	5.4
2SRA	3.4	13.1	6.3	8.1
0.5SAP	4.1	15.1	3.9	12.3
10EA2SRA	3.5	14.4	5.3	5.0
10EA0.5SAP	4.2	21.5	4.0	2.0
2SRA0.5SAP	4.3	17.0	3.7	11.1
10EA2SRA0.5SAP	4.0	17.6	3.4	6.1

3.7. Internal relative humidity

Fig. 11 shows the effect of single SMM on relative humidity (RH) of FRM mixtures. The highest and lowest RH within 10 days were exhibited by the 0.5SAP and 10EA mixtures. The incorporation of SAP absorbed water in the mixture and reduced the initial RH to around 75% immediately after casting the sample, however, after a day and half the mixture's RH reached 100%. That is because, immediately after casting, ion concentration in SAP particles is higher, and it causes the matrix' water to flow to SAP particles. However, after hydration the ion concentration of matrix increases, and the reverse water flow occurs [62,63]. Therefore, the 0.5SAP mixture's RH started to drop after 3.5 days and reached 89% after 10 days. The use of SRA in the 2SRA mixture resulted in almost no RH drop immediately after casting the sample. However, after three days the RH started to reduce and reached 86% at 10 days. The effectiveness of SRA in enhancing RH was elaborated in previous studies [8,54,64]. The use of 10% EA resulted in quicker drop of RH and the lowest final RH of 81%. This was due to high water absorption of the 10EA mixture for the hydration of CaO. In addition, based on the hydration kinetics discussed in 3.5, EA accelerates hydration leading to lower RH and higher self-desiccation. This phenomenon was discussed in previous studies [65,66].

3.8. XRD analysis

Fig. 12 shows the XRD pattern, and Table 12 summarizes the semi-quantitative analysis of the crystalline phases for the main FRM mixtures at 28 days. The provided analysis in Table 12 indicates that the highest CH was obtained by the mixtures made with EA, which led to a significant initial expansion. The higher intensity of CH peaks in the coupled mixtures containing EA, can represent the higher expansion of these systems as was shown in Fig. 8b. The highest amount of unhydrated phases was recorded for the 2SRA mixture, which could be associated with the postponing hydration effect of SRA. The combined use of SMM led to 18% lower un-hydrated phases. This implies the coupled effect of SMM in hydration development, which resulted in more hydration products and expansion at the presence of EA. The SiO_2 peaks shown in Fig. 12 were prominent for the REF, 0.5SAP, and 2SRA0.5SAP mixtures, as confirmed by Table 12.

3.9. BSEM observation at fiber-matrix interface

3.9.1. Morphology observation

BSEM images showing the microstructure of the investigated mixtures made with single SMM at the interface of fiber and matrix are presented in Fig. 13. The scanning was performed surrounding up to 10 fibers, and all were compared to realize the common pattern. The images

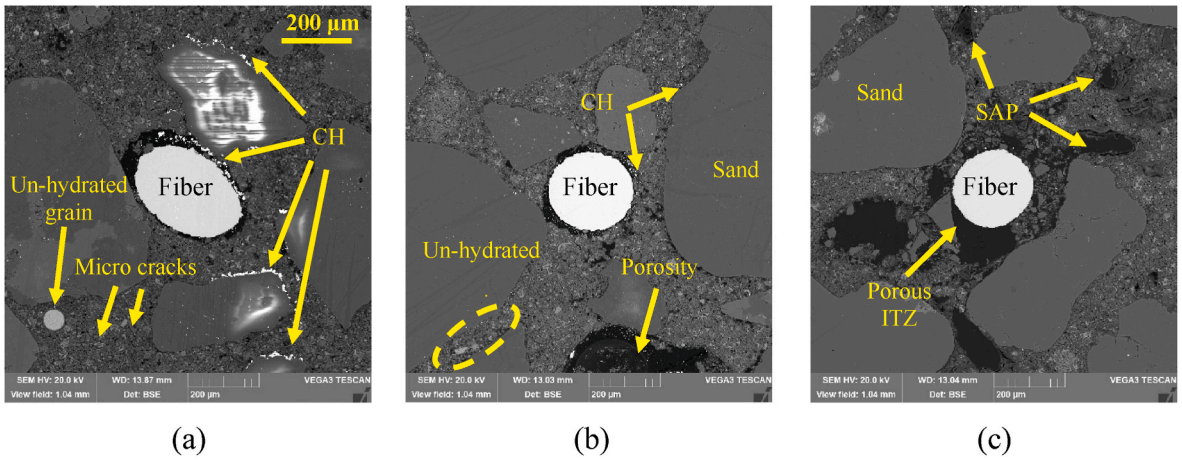

Fig. 13. BSEM images of (a) 10EA; (b) 2SRA; (c) 0.5SAP mixtures at fiber-matrix interface.

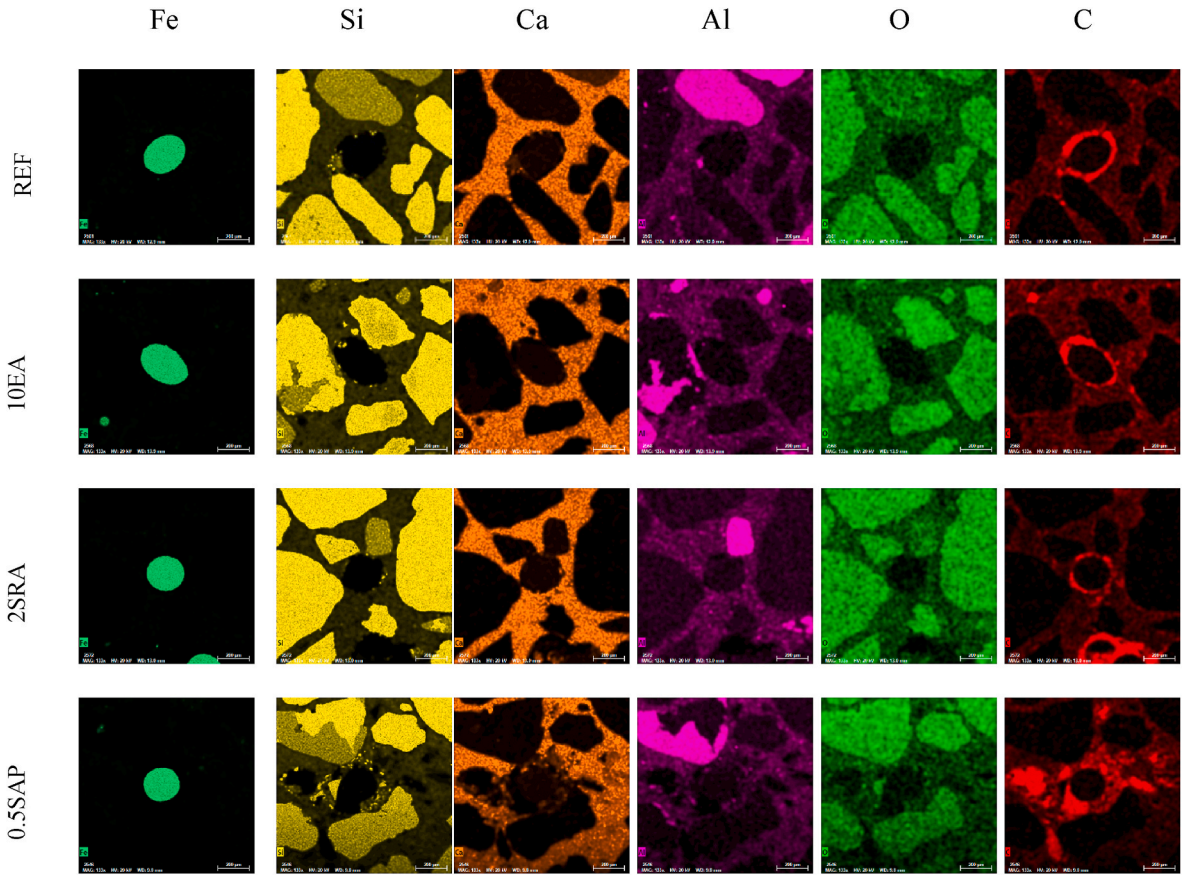

Fig. 14. Element-mapping at interface of fiber and matrix of FRM mixtures made with a single SMM.

shown in Fig. 13 are representative of the samples. Brighter spots correspond to un-hydrated binder and dark spots in the cement matrix indicate the presence of hydration products. As shown in Fig. 13a, the presence of CH which deposited around voids and at aggregate-matrix ITZ is very prominent in the 10EA mixtures. The amount of un-hydrated grains for the 2SRA mixture is relatively higher than other mixtures. This agrees with the XRD analysis results. As observed and reported in previous studies the use of SRA contributed to the creation of large pores into the matrix (Fig. 13b) [53,67]. Fig. 13c shows high porosity for the 0.5SAP mixture compared to the other mixtures, especially at the fiber-matrix ITZ. This higher porosity surrounding the fiber contributes to lower fiber pull-out characteristics for this mixture, which was reported in section 3.2.

3.9.2. *Energy dispersive spectroscopy (EDS) micro analysis*

Fig. 14 displays element mapping at fiber-matrix interface, which provides the distribution of Fe, C, Ca, Si, Al, and O at the vicinity of fiber for the investigated mixtures made with a single SMM. The green area in the middle identifies steel fiber. The Si signifies sand particles and silica in hydration products. The C indicates porosity. The other elements are representative of hydration products. The brighter spots refer to the greater and purer content of the element. As can be seen, the C (red

region) refers to porosity and voids into the matrix and can reflect mechanical properties. The C is dominant for the 0.5SAP mixture due to the presence of voids from swelled SAP particles after desorption. Lower porosity can be found for the REF and 2SRA mixtures indicating higher strength and fiber-matrix bonding. The higher quantity of Ca in the 10EA mixture is dominant, which contributes to higher CH formation at the presence of EA.

4. Conclusions

In this paper a statistical factorial design was developed to evaluate the combined effect of CaO-based EA, SRA, and SAP on compressive strength development, fiber pull-out, and shrinkage of FRM mixtures. Hydration kinetics, variation of IRH, and microstructural characterization were carried out to further evaluate the effect of SMM on the performance of FRM. Based on the obtained results, the following conclusions can be drawn:

1. In the coupled systems of SMM in FRM, SMM can be recommended to be limited to 5% EA, 1% SRA, and 0.5% SAP.
2. The preferred SMM combination considering compressive strength, fiber pull-out strength, and shrinkage was the coupled system of EA and SRA.
3. High heat of hydration obtained using 10% EA in the corresponding mixtures confirmed excessive CH formation and high expansion, which adversely affected the mechanical properties.
4. The use of 0.5% SAP with additional water contributed to the excessive expansion of the SAP particles (at least seven times), which created voids into the matrix leading to lower compressive strength and fiber-matrix bonding.
5. A multi-objective optimization based on the measured properties was performed. The results revealed that the individual use of 7.5% EA and coupled use of 5% EA either with 0.5% SRA or 0.125% SAP can result in producing flowable, high strength, and low shrinkage FRM mixtures, which can be employed for repair applications.

Declaration of competing interest

The authors declare that they have no known competing financial interests or personal relationships that could have appeared to influence the work reported in this paper.

Data availability

No data was used for the research described in the article.

References

[1] M. Sarigaphuti, S.P. Shah, K.D. Vinson, Shrinkage cracking and durability characteristics of cellulose fiber reinforced concrete, ACI Mater. J. 90 (4) (1993).

[2] K. Kawaai, I. Ujike, I. Nakai, Effects of Internal Cracking and Drying Shrinkage on the Corrosion Processes of RC Beam Specimens, 2015, pp. 477–486, https://doi.org/10.1061/9780784479346.057.

[3] F.U.A. Shaikh, Effect of cracking on corrosion of steel in concrete, Int. J. Concr. Struct. Mater. 12 (1) (2018) 3, https://doi.org/10.1186/s40069-018-0234-y.

[4] K.A. Sakata, Study on moisture diffusion in drying and drying shrinkage of concrete, Cement Concr. Res. 13 (2) (1983) 216–224, https://doi.org/10.1016/0008-8846(83)90104-7.

[5] Jang, S.-J.; Kim, S.-W.; Park, W.-S.; Kobayashi, K.; Yun, H.-D. Effects of Shrinkage-Compensation on Mechanical Properties and Repair Performance of Strain-Hardening Cement Composite Materials. Adv. Civ. Eng.. https://www.hindawi.com/journals/ace/2018/6727516/(accessed 2020-08-09). https://doi.org/10.1155/2018/6727516.

[6] T. Xie, C. Fang, M.S. Mohamad Ali, P. Visintin, Characterizations of autogenous and drying shrinkage of ultra-high performance concrete (UHPC): an experimental study, Cement Concr. Compos. 91 (2018) 156–173, https://doi.org/10.1016/j.cemconcomp.2018.05.009.

[7] V. Mechtcherine, D. Snoeck, C. Schröfl, N. De Belie, A.J. Klemm, K. Ichimiya, J. Moon, M. Wyrzykowski, P. Lura, N. Toropovs, A. Assmann, S. Igarashi, I. De La Varga, F.C.R. Almeida, K. Erk, A.B. Ribeiro, J. Custódio, H.W. Reinhardt, V. Falikman, Testing superabsorbent polymer (SAP) sorption properties prior to implementation in concrete: results of a RILEM round-robin test, Mater. Struct. 51 (1) (2018) 28, https://doi.org/10.1617/s11527-018-1149-4.

[8] F. Rajabipour, G. Sant, J. Weiss, Interactions between shrinkage reducing admixtures (SRA) and cement paste's pore solution, Cement Concr. Res. 38 (5) (2008) 606–615, https://doi.org/10.1016/j.cemconres.2007.12.005.

[9] S.-H. Kang, S.-G. Hong, J. Moon, The effect of superabsorbent polymer on various scale of pore structure in ultra-high performance concrete, Construct. Build. Mater. 172 (2018) 29–40, https://doi.org/10.1016/j.conbuildmat.2018.03.193.

[10] D. Snoeck, D. Schaubroeck, P. Dubruel, N. De Belie, Effect of high amounts of superabsorbent polymers and additional water on the workability, microstructure and strength of mortars with a water-to-cement ratio of 0.50, Construct. Build. Mater. 72 (2014) 148–157, https://doi.org/10.1016/j.conbuildmat.2014.09.012.

[11] M.T. Hasholt, O.M. Jensen, K. Kovler, S. Zhutovsky, Can superabsorent polymers mitigate autogenous shrinkage of internally cured concrete without compromising the strength? Construct. Build. Mater. 31 (2012) 226–230, https://doi.org/10.1016/j.conbuildmat.2011.12.062.

[12] W. Shi, M. Najimi, B. Shafei, Chloride penetration in shrinkage-compensating cement concretes, Cement Concr. Compos. 113 (2020), 103656, https://doi.org/10.1016/j.cemconcomp.2020.103656.

[13] R. Hassanli, O. Youssf, T. Vincent, J.E. Mills, A. Manalo, R. Gravina, Experimental study on compressive behavior of FRP-confined expansive rubberized concrete, J. Compos. Construct. 24 (4) (2020), 04020034, https://doi.org/10.1061/(ASCE)CC.1943-5614.0001038.

[14] S. Gao, Z. Wang, W. Wang, H. Qiu, Effect of shrinkage-reducing admixture and expansive agent on mechanical properties and drying shrinkage of engineered cementitious composite (ECC), Construct. Build. Mater. 179 (2018) 172–185, https://doi.org/10.1016/j.conbuildmat.2018.05.203.

[15] L. Mo, M. Deng, M. Tang, Effects of Calcination Condition on Expansion Property of MgO-type Expansive Agent Used in Cement-Based Materials, 2010, https://doi.org/10.1016/J.CEMCONRES.2009.09.025.

[16] L. Mo, F. Zhang, D.K. Panesar, M. Deng, Development of low-carbon cementitious materials via carbonating portland cement–fly ash–magnesia blends under various curing scenarios: a comparative study, J. Clean. Prod. 163 (2017) 252–261, https://doi.org/10.1016/j.jclepro.2016.01.066.

[17] L. Mo, F. Zhang, M. Deng, D.K. Panesar, Effectiveness of using CO2 pressure to enhance the carbonation of portland cement-fly ash-MgO mortars, Cement Concr. Compos. 70 (2016) 78–85, https://doi.org/10.1016/j.cemconcomp.2016.03.013.

[18] R. Polat, R. Demirboğa, W.H. Khushefati, Effects of nano and micro size of CaO and MgO, nano-clay and expanded perlite aggregate on the autogenous shrinkage of mortar, Construct. Build. Mater. 81 (2015) 268–275, https://doi.org/10.1016/j.conbuildmat.2015.02.032.

[19] L. Yang, C. Shi, Z. Wu, Mitigation techniques for autogenous shrinkage of ultra-high-performance concrete – a review, Compos. B Eng. 178 (2019), 107456, https://doi.org/10.1016/j.compositesb.2019.107456.

[20] O.M. Jensen, Water absorption of superabsorbent polymers in a cementitious environment: international conference on advances in construction materials through science and engineering, in: International RILEM Conference on Advances in Construction Materials through Science and Engineering 2011, 2011.

[21] C. Schröfl, K.A. Erk, W. Siriwatwechakul, M. Wyrzykowski, D. Snoeck, Recent progress in superabsorbent polymers for concrete, Cement Concr. Res. 151 (2022), 106648, https://doi.org/10.1016/j.cemconres.2021.106648.

[22] M. Wyrzykowski, S.-I. Igarashi, P. Lura, V. Mechtcherine, Recommendation of RILEM TC 260-RSC: using superabsorbent polymers (SAP) to mitigate autogenous shrinkage, Mater. Struct. 51 (5) (2018) 135, https://doi.org/10.1617/s11527-018-1241-9.

[23] L.P. Esteves, On the absorption kinetics of superabsorbent polymers, Int. RILEM Conf. Use Superabsorbent Polym. (2010) 77–84.

[24] V. Mechtcherine, E. Secrieru, C. Schröfl, Effect of superabsorbent polymers (SAPs) on rheological properties of fresh cement-based mortars — development of yield stress and plastic viscosity over time, Cement Concr. Res. 67 (2015) 52–65, https://doi.org/10.1016/j.cemconres.2014.07.003.

[25] M. Wyrzykowski, P. Lura, Controlling the coefficient of thermal expansion of cementitious materials – a new application for superabsorbent polymers, Cement Concr. Compos. 35 (1) (2013) 49–58, https://doi.org/10.1016/j.cemconcomp.2012.08.010.

[26] M. Valipour, K.H. Khayat, Coupled effect of shrinkage-mitigating admixtures and saturated lightweight sand on shrinkage of UHPC for overlay applications, Construct. Build. Mater. 184 (2018) 320–329, https://doi.org/10.1016/j.conbuildmat.2018.06.191.

[27] V. Mechtcherine, M. Gorges, C. Schroefl, A. Assmann, W. Brameshuber, A. B. Ribeiro, D. Cusson, J. Custódio, E.F. da Silva, K. Ichimiya, S. Igarashi, A. Klemm, K. Kovler, A.N. de Mendonça Lopes, P. Lura, V.T. Nguyen, H.-W. Reinhardt, R.D. T. Filho, J. Weiss, M. Wyrzykowski, G. Ye, S. Zhutovsky, Effect of internal curing by using superabsorbent polymers (SAP) on autogenous shrinkage and other properties of a high-performance fine-grained concrete: results of a RILEM round-robin test, Mater. Struct. 47 (3) (2014) 541–562, https://doi.org/10.1617/s11527-013-0078-5.

[28] J. Yang, F. Wang, X. He, Y. Su, Pore structure of affected zone around saturated and large superabsorbent polymers in cement paste, Cement Concr. Compos. (2019), https://doi.org/10.1016/J.CEMCONCOMP.2018.12.020.

[29] J. Liu, N. Farzadnia, C. Shi, Effects of superabsorbent polymer on interfacial transition zone and mechanical properties of ultra-high performance concrete, Construct. Build. Mater. 231 (2020), 117142, https://doi.org/10.1016/j.conbuildmat.2019.117142.

[30] V. Mechtcherine, M. Wyrzykowski, C. Schröfl, D. Snoeck, P. Lura, N. De Belie, A. Mignon, S. Van Vlierberghe, A.J. Klemm, F.C.R. Almeida, J.R. Tenório Filho, W.

P. Boshoff, H.-W. Reinhardt, S.-I. Igarashi, Application of super absorbent polymers (SAP) in concrete construction—update of RILEM state-of-the-art report, Mater. Struct. 54 (2) (2021) 80, https://doi.org/10.1617/s11527-021-01668-z.
[31] A. Pourjavadi, S.M. Fakoorpoor, A. Khaloo, P. Hosseini, Improving the performance of cement-based composites containing superabsorbent polymers by utilization of nano-SiO2 particles, Mater. Des. 42 (2012) 94–101, https://doi.org/10.1016/j.matdes.2012.05.030.
[32] S. Zhutovsky, K. Kovler, A. Bentur, Influence of Cement Paste Matrix Properties on the Autogenous Curing of High-Performance Concrete, 2004, https://doi.org/10.1016/S0958-9465(03)00082-9.
[33] G. Lefever, E. Tsangouri, D. Snoeck, D.G. Aggelis, N. De Belie, S. Van Vlierberghe, D. Van Hemelrijck, Combined use of superabsorbent polymers and nanosilica for reduction of restrained shrinkage and strength compensation in cementitious mortars, Construct. Build. Mater. 251 (2020), 118966, https://doi.org/10.1016/j.conbuildmat.2020.118966.
[34] Y. Wehbe, A. Ghahremaninezhad, Combined effect of shrinkage reducing admixtures (SRA) and superabsorbent polymers (SAP) on the autogenous shrinkage, hydration and properties of cementitious materials, Construct. Build. Mater. 138 (2017) 151–162, https://doi.org/10.1016/j.conbuildmat.2016.12.206.
[35] L. De Meyst, E. Mannekens, M. Araújo, D. Snoeck, K. Van Tittelboom, S. Van Vlierberghe, N. De Belie, Parameter study of superabsorbent polymers (SAPs) for use in durable concrete structures, Materials 12 (9) (2019) 1541, https://doi.org/10.3390/ma12091541.
[36] Solving shrinkage problem of ultra-high-performance concrete by a combined use of expansive agent, super absorbent polymer, and shrinkage-reducing agent, Compos. B Eng. 230 (2022), 109503, https://doi.org/10.1016/j.compositesb.2021.109503.
[37] D. Snoeck, C. Schröfl, V. Mechtcherine, Recommendation of RILEM TC 260-RSC: testing sorption by superabsorbent polymers (SAP) prior to implementation in cement-based materials, Mater. Struct. 51 (5) (2018) 116, https://doi.org/10.1617/s11527-018-1242-8.
[38] D. Snoeck, L. Pel, N. De Belie, The water kinetics of superabsorbent polymers during cement hydration and internal curing visualized and studied by NMR, Sci. Rep. 7 (1) (2017) 9514, https://doi.org/10.1038/s41598-017-10306-0.
[39] ASTM C1761. Standard Specification for Lightweight Aggregate for Internal Curing of Concrete.
[40] ASTM Committee C09, A. W. New Test Method for Measurement of Fresh Hydraulic Cement Paste Spread Using a Mini-Slump Cone, 2018.
[41] ASTM C109/C109M-20, A. C. Standard Test Method for Compressive Strength of Hydraulic Cement Mortars (Using 2-in. Or [50-Mm] Cube Specimens); ASTM International, West Conshohocken, PA.
[42] Z. Wu, K.H. Khayat, C. Shi, B.F. Tutikian, Q. Chen, Mechanisms underlying the strength enhancement of UHPC modified with nano-SiO2 and nano-CaCO3, Cement Concr. Compos. 119 (2021), 103992, https://doi.org/10.1016/j.cemconcomp.2021.103992.
[43] ASTM C157, Test Method for Length Change of Hardened Hydraulic-Cement Mortar and Concrete, ASTM International, 2017, https://doi.org/10.1520/C0157_C0157M-17.
[44] S. Zuo, Q. Yuan, T. Huang, M. Zhang, Q. Wu, Rheological behaviour of low-heat portland cement paste with MgO-based expansive agent and shrinkage reducing admixture, Construct. Build. Mater. 304 (2021), 124583, https://doi.org/10.1016/j.conbuildmat.2021.124583.
[45] M. Deng, D. Hong, X. Lan, M. Tang, Mechanism of expansion in hardened cement pastes with hard-burnt free lime, Cement Concr. Res. 25 (2) (1995) 440–448, https://doi.org/10.1016/0008-8846(95)00030-5.
[46] J. Dang, J. Zhao, Z. Du, Effect of superabsorbent polymer on the properties of concrete, Polymers 9 (12) (2017), https://doi.org/10.3390/polym9120672.
[47] W. Zuo, P. Feng, P. Zhong, Q. Tian, N. Gao, Y. Wang, C. Yu, C. Miao, Effects of novel polymer-type shrinkage-reducing admixture on early age autogenous deformation of cement pastes, Cement Concr. Res. 100 (2017) 413–422, https://doi.org/10.1016/j.cemconres.2017.08.007.
[48] A.E. Klausen, T. Kanstad, The effect of shrinkage reducing admixtures on drying shrinkage, autogenous deformation, and early age stress development of concrete, Struct. Concr. 22 (S1) (2021) E596–E606, https://doi.org/10.1002/suco.201900583.
[49] K. Farzanian, K. Pimenta Teixeira, I. Perdigão Rocha, L. De Sa Carneiro, A. Ghahremaninezhad, The mechanical strength, degree of hydration, and electrical resistivity of cement pastes modified with superabsorbent polymers, Construct. Build. Mater. 109 (2016) 156–165, https://doi.org/10.1016/j.conbuildmat.2015.12.082.
[50] K. Aghaee, K.H. Khayat, Effect of shrinkage-mitigating materials on performance of fiber-reinforced concrete – an overview, Construct. Build. Mater. 305 (2021), 124586, https://doi.org/10.1016/j.conbuildmat.2021.124586.
[51] K. Aghaee, N. Farzadnia, K.H. Khayat, Coupled effect of expansive agent and curing on mechanical and shrinkage properties of fiber-reinforced eco-crete, Construct. Build. Mater. 310 (2021), 125285, https://doi.org/10.1016/j.conbuildmat.2021.125285.
[52] M. Kioumarsi, F. Azarhomayun, M. Haji, M. Shekarchi, Effect of shrinkage reducing admixture on drying shrinkage of concrete with different w/c ratios, Materials (Basel) 13 (24) (2020), https://doi.org/10.3390/ma13245721.
[53] V. Bílek, L. Kalina, R. Novotný, J. Tkacz, L. Pařízek, Some issues of shrinkage-reducing admixtures application in alkali-activated slag systems, Materials (Basel) 9 (6) (2016) 462, https://doi.org/10.3390/ma9060462.
[54] D.P. Bentz, Influence of shrinkage-reducing admixtures on early-age properties of cement pastes, J. Adv. Concr. Technol. 4 (3) (2006) 423–429, https://doi.org/10.3151/jact.4.423.
[55] S. Zuo, Q. Yuan, T. Huang, M. Zhang, Q. Wu, Rheological behaviour of low-heat portland cement paste with MgO-based expansive agent and shrinkage reducing admixture, Construct. Build. Mater. 304 (2021), 124583, https://doi.org/10.1016/j.conbuildmat.2021.124583.
[56] J. Guo, S. Zhang, T. Guo, P. Zhang, Effects of UEA and MgO expansive agents on fracture properties of concrete, Construct. Build. Mater. 263 (2020), 120245, https://doi.org/10.1016/j.conbuildmat.2020.120245.
[57] M. Collepardi, A. Borsoi, S. Collepardi, J.J. Ogoumah Olagot, R. Troli, Effects of shrinkage reducing admixture in shrinkage compensating concrete under non-wet curing conditions, Cement Concr. Compos. 27 (6) (2005) 704–708, https://doi.org/10.1016/j.cemconcomp.2004.09.020.
[58] K. Aghaee, R. Sposito, K.H. Khayat, Synergistic effect of shrinkage mitigating materials on rheological properties of flowable and thixotropic cement paste, Cement Concr. Compos. (2022), 104686, https://doi.org/10.1016/j.cemconcomp.2022.104686.
[59] V. Corinaldesi, Combined effect of expansive, shrinkage reducing and hydrophobic admixtures for durable self compacting concrete, Construct. Build. Mater. 36 (2012) 758–764, https://doi.org/10.1016/j.conbuildmat.2012.04.129.
[60] Design and Analysis of Experiments, tenth ed. | *Wiley*. Wiley.com. https://www.wiley.com/en-us/Design+and+Analysis+of+Experiments%2C+10th+Edition-p-9781119492443 (accessed 2021-02-22).
[61] JMP 12 Design of Experiments Guide [Book]. https://www.oreilly.com/library/view/jmp-12-design/9781629594422/(accessed 2021-11-14).
[62] O.M. Jensen, P.F. Hansen, Water-entrained cement-based materials: I. Principles and theoretical background, Cement Concr. Res. 31 (4) (2001) 647–654, https://doi.org/10.1016/S0008-8846(01)00463-X.
[63] A.M. Soliman, M.L. Nehdi, Effect of drying conditions on autogenous shrinkage in ultra-high performance concrete at early-age, Mater. Struct. 44 (5) (2011) 879–899, https://doi.org/10.1617/s11527-010-9670-0.
[64] D.P. Bentz, Curing with shrinkage-reducing admixtures, Concr. Int. 55 (2005).
[65] E. Tazawa (Ed.), Autogenous Shrinkage of Concrete, CRC Press, London, 2014, https://doi.org/10.1201/9781482272123.
[66] P. Shen, L. Lu, Y. He, F. Wang, J. Lu, H. Zheng, S. Hu, Investigation on expansion effect of the expansive agents in ultra-high performance concrete, Cement Concr. Compos. 105 (2020), 103425, https://doi.org/10.1016/j.cemconcomp.2019.103425.
[67] L. Coppola, D. Coffetti, E. Crotti, S. Candamano, F. Crea, G. Gazzaniga, T. Pastore, The combined use of admixtures for shrinkage reduction in one-Part Alkali activated slag-based mortars and pastes, Construct. Build. Mater. 248 (2020), 118682, https://doi.org/10.1016/j.conbuildmat.2020.118682.